Colloids and Surfaces B: Biointerfaces 190 (2020) 110981

Contents lists available at ScienceDirect

Colloids and Surfaces B: Biointerfaces

journal homepage: www.elsevier.com/locate/colsurfb

# Bioelectrocatalysis and surface analysis of gold coated with nickel oxide/hydroxide and glucose oxidase towards detection of glucose

Nqobile Njoko[a], Marcel Louzada[a], Jonathan Britton[a,b], Samson Khene[a], Tebello Nyokong[a,b], Philani Mashazi[a,b,*]

[a] Chemistry Department, P.O. Box 94, Makhanda, 6140, South Africa
[b] Institute for Nanotechnology Innovation, Rhodes University, P.O. Box 94, Makhanda, 6140, South Africa

ARTICLE INFO

*Keywords:*
Nickel oxide/hydroxide
Thin films
Glucose oxidase
Hydrogen peroxide
Bioelectrocatalysis

ABSTRACT

The fabricating of metal oxide thin films onto conducting surfaces continues to grow and their potential applications as surfaces for biosensor applications is of paramount importance. The correct orientation of glucose oxidase redox enzymes yields very important biointerfaces capable of selectively detecting D-glucose as a measure of blood sugar for healthy and diabetic sick patients. The electrodeposition of redox enzymes, such as glucose oxidase enzymes, onto gold electrode surfaces pre-modified with nickel oxide was investigated in this work. The surface characterization confirmed the chemical nature, morphology and thin film composition of the modification of bare and modified gold electrodes. The electrodeposition of GOx enzyme onto nickel oxide/hydroxide thin film resulted in a surface with excellent bioelectrocatalytic properties towards the detection of D-glucose. The nickel within the nickel oxide/hydroxide thin film had a Ni(II) oxidation state. A well-defined redox peak of GOx enzyme co-factor ($FAD/FADH_2$) was observed confirming the oriented immobilization onto NiO/$Ni(OH)_2$ conducting surfaces. The amount of GOx enzyme deposited was determined by integrating the charge (Q = 0.368 μF) under the reduction peak and the surface coverage was found to be $1.43 \times 10^{-10}$ mol. $cm^{-2}$. A linear plot of electrocatalytic reduction currents against D-glucose concentrations was obtained up to 30.0 mM with a linear correlation coefficient ($R^2$) of 0.99. The limit of detection (LoD) using S/N = 3 was calculated to be 1.54 ± 0.03 mM. The sensitivity of the biosensors was 1.95 ± 0.13 μA.mM.$cm^{-2}$. The selectivity towards only D-glucose and not ascorbic acid and uric acid was evaluated and the Au-NiO/$Ni(OH)_2$-GOx could not detect 1.0 mM of ascorbic acid and uric acid.

## 1. Introduction

The interest in bioelectrochemical sensors has increased over the years due to their advantages, such as sensitivity and selectivity, fast response, easy operation and continuous on-line detection. Biosensors have been of interest in various fields, particularly in biochemistry, environmental monitoring and clinical diagnosis [1]. Glucose-based biosensors are the most widely studied and commercially available systems. They have been used for the detection of glucose in clinical, biological, chemical samples and food processing and fermentation [1,2]. This highlights the variety of media where glucose can be detected and hence the continued demand for glucose biosensors. Repetitive analysis in a variety of physiological fluids is one of the most vital and frequent processes in a clinical laboratories [3–8]. Glucose is an important analyte or biomolecule in the human metabolism processes [8,9]. Patients with diabetes are required to monitor blood glucose levels daily. This has led to a growing demand of glucose monitoring biosensors. Therefore, glucose biosensors that are selective, reliable, cheap and easy to operate for continuous monitoring of glucose levels are of importance [5–7].

Biosensors require modification of electrode surfaces with enzymes impart some selectivity and specificity towards the analyte of interest [1,2,9–12]. The challenge is that redox enzymes, such as glucose oxidase, peroxidase, and laccase do not readily exchange electrons with the solid electrode surfaces [13–20]. This is because the redox cofactor such as FAD (flavin adenine dinucleotide), iron porphyrin (Heme), NAD (nicotinamide adenine dinucleotide) are embedded within the large 3D glycoprotein with complex structures. The redox enzyme 3D glycoprotein hinders optimum interaction and electron transfer with the electrode surface [10]. Modification of electrode surfaces is the method used for improving biomolecular interaction with solid electrode surfaces. Different types materials such as carbon nanotubes, metal oxides

* Corresponding author at: Chemistry Department, P.O. Box 94, Makhanda, 6140, South Africa.
*E-mail address:* P.Mashazi@ru.ac.za (P. Mashazi).

https://doi.org/10.1016/j.colsurfb.2020.110981
Received 14 December 2019; Received in revised form 12 March 2020; Accepted 15 March 2020
Available online 16 March 2020

and polymer composites as electrode modifiers has to some extent achieved direct electron transfer between redox enzymes and electrode surfaces [13–19]. Metal oxides have been widely used to improve the development of electrochemical biosensors [10,21,22]. Nickel oxide used in this work is a p-type semiconductor with wide band gap ranging from 3.6 to 4.0 eV and a large exciton binding energy [23]. Different techniques have been used for the preparation of $NiO/Ni(OH)_2$ and for electrochemical applications. Most common methods involve sol-gel preparation of powder nickel oxide followed by casting, electrodeposition [11,12]. The electrodeposition method was used in this work to deposit Ni and form it oxides on the surface of gold electrode. Nickel exhibits excellent electrocatalytic activity due to the Ni-O-Ni (nickel oxo-bridge) in alkaline medium. The nickel (electronic configuration) has vacant D-orbitals with unpaired electrons arising from the oxidized form of nickel oxide/hydroxide, $NiO/Ni(OH)_2$. This allows for nickel oxide/hydroxide to readily bind with adsorbed biomolecules [22]. Nickel oxide/hydroxides as an excellent capacitor was investigated on carbon-based electrodes [24–31].

This study investigates the modification of gold electrodes (using the electrodeposition method) with $NiO/Ni(OH)_2$ thin films to provide conducive environment for the immobilization glucose oxidase (GOx) enzyme. The electrodeposition of Ni onto gold surface has not been thoroughly studied with just one report published thus far [32]. The modified gold electrode surfaces with $NiO/Ni(OH)_2$ and $NiO/Ni(OH)_2$-GOx thin films were investigated for $H_2O_2$ and glucose detection. Gold electrode was used in this work, due to the ease with which the $NiO/Ni(OH)_2$ electrodeposition was achieved at relatively low reduction potentials compared with high reduction potentials on the glassy carbon electrode. The nickel under-potential deposition (NiUDP) onto gold surface was converted to electroactive $NiO/Ni(OH)_2$ in alkaline medium. The surface analysis and characterization using surface sensitive techniques confirmed the electrodeposited materials. This is the novelty of the current work and to our best knowledge this is for the first time reported.

## 2. Experimental

### 2.1. Materials and methods

Glucose oxidase (EC 1.1.3.4. Type II: from *Aspergillus niger*), Nickel nitrate hexahydrate [$Ni(NO_3)_2.6H_2O$] and D-glucose were purchased from Sigma. The stock solution containing 5.0 $\mu g.mL^{-1}$ GOx solutions (pH 7.4) was prepared and stored at 4 °C. The phosphate buffer solutions (PBS, 1.0 mM) was prepared from $K_2HPO_4$ and the pH was adjusted to the required value (pH 7.4) with HCl and KOH solutions. Ni $(NO_3)_2{\cdot}6H_2O$ and other reagents used were of analytical reagent grade. Pure argon was used to purge the solution to remove dissolved oxygen and a blanket of argon was maintained during the experiments.

Electrochemical experiments were performed using the experimental setup as previously reported [33]. Briefly, a computer controlled Autolab modular electrochemical system (EcoChemie) was driven by GPES software. Gold disk electrode purchase from BASi Inc was used as a working electrode (WE, 1.6 mm diameter) and platinum wire as auxiliary/counter electrode (CE) and silver-silver chloride (Ag|AgCl in 3 M NaCl) as the reference electrode (RE). The gold disc electrode from BASi Inc does not fit within the sample analysis chamber and sample holder of spectroscopic and microscopic analysis techniques. A flat gold coated quartz crystals (AuCQC, O100RX1, 5 MHz) purchased from Stanford Research Systems (SRS) were used for X-ray Photoelectron Spectroscopy (XPS), Atomic Force Microscopy (AFM) and Time-of-Flight Secondary Ion Mass Spectrometry (TOF-SIMS) analysis. The XPS analysis and instrumental setup were as previously reported [34,35]. The peak fitting was achieved using the Vision Processing data reduction software from Kratos Analytical LTD was used for peak synthesis and fitting. The NIST XPS Database [36] was used for peak assignments. The atomic force microscope images were recorded using an Asylum Research MFP-3D Classic (Santa Barbara, USA) in AC mode. The TOF-SIMS experimental setup was as reported before [37]. All experiments were carried out using high purity water from a Millipore (Milli-Q System) with resistivity of 18.2 MΩ.cm at ambient temperature of 25°C.

### 2.2. Preparation of nickel oxide/hydroxide-glucose oxidase thin film

The electrodeposition of nickel thin film onto the gold electrode surface was carried out using an optimized constant cathodic potential of -0.80 V in pH 4.0 acetate buffer solution containing 1.0 mM nickel nitrate, $Ni(NO_3)_2.6H_2O$. The potential established by cyclic voltammetry scan which showed reduction of Ni(II) to Ni(0) in two steps and underpotential deposition of nickel (NiUDP) as an adatom. Chronoamperometry was used for the controlled electrodeposition of Ni and GOx enzyme thin films. The electrodeposition times were varied from $5-20$ min and the optimum conditions with high electrocatalytic currents used. Au-Ni thin films were washed with acetate buffer and finally with copious amounts of ultra-pure water to remove the physically absorbed nickel nitrate from the gold electrode. The nickel thin film was converted to nickel oxide/hydroxide ($NiO/Ni(OH)_2$) by cycling multiple times in 0.10 M NaOH between -0.20 to $+0.50$ V (vs Ag|AgCl 3.0 M NaCl). The modified gold electrode was represented as Au-$NiO/Ni(OH)_2$. The Au-$NiO/Ni(OH)_2$ was used for the electrodeposition of GOx enzyme. Au-$NiO/Ni(OH)_2$ electrode was immersed into a freshly prepared phosphate buffer solution (PBS, pH 7.4) containing 5.0 $\mu g.mL^{-1}$ of GOx in 2.0 mL. Constant anodic potential was applied ($+0.80$ V vs Ag|AgCl 3.0 NaCl) for 15 min (or until stable chronoamperommogram signal was obtained). This resulted in the electrodeposition and immobilization of GOx enzyme onto the Au-$NiO/Ni(OH)_2$. The GOx modified gold electrode surface was represented as Au-$NiO/Ni(OH)_2$-GOx.

## 3. Results and discussion

### 3.1. Electrodeposition of $NiO/Ni(OH)_2$ and GOx thin film on the Au surface

A cyclic voltammetry (CV) of the nickel nitrate solution was recorded to investigate the potential at which nickel is reduced onto the gold electrode. Fig. 1 shows (a) cyclic voltammogram of gold electrode measured between 0.60 V to $-1.0$ V in pH 4.0 acetate buffer solution containing 1.0 mM $Ni(NO_3)_2.6H_2O$ and (b) chronoamperommogram for the electrodeposition of Ni(0) onto gold surface. The cyclic voltammogram in Fig. 1(a) exhibited a peak at –0.33 V labelled (**I**) corresponding to the reduction of Ni(II) to Ni(I), $Ni(II) + e^- \leftrightarrow Ni(I)$. An additional reduction peak at -0.70 V labelled (**II**) was observed and due to the reduction of N(I) to Ni(0), $Ni(I) + e^- \leftrightarrow Ni(0)$. When the potential was scanned to a more negative potential an additional peak at $-0.77$ V labelled with an asterisk (*) was observed and due to the non-faradaic adsorption of Ni(0) onto gold surface forming an Au-Ni adatom. The anodic scan exhibited an oxidation of Ni(0) to Ni(I) peak labelled (**III**). This showed as multiple peaks due to the stripping of Ni and oxidation of Ni(0) to Ni(I) simultaneously dissolving back into the solution. Additional oxidation peaks were observed and labelled (**IV**) due to Ni(I) oxidation to Ni(II). From this investigation, the electrodeposition potential was obtained as $-0.77$ V. An overpotential of -0.80 V was used for the electrodeposition of Ni onto gold electrode surface, in Fig. 1(b). This experiment is well-known for copper deposition on gold, that is, copper underpotential deposition (CuUDP) [38].

Chronoamperometry was used for the electrodeposition of Ni onto gold electrode surface and the applied potential of $-0.80$ V was used. There was a current decreased with time, as the nickel layer was electrodeposited onto the gold electrode. Electrodeposition of a metal on a different metal substrate results in a formation of an ad-atom. For example, nickel electrodeposition onto gold resulted in the formation of nickel-gold (Au-Ni) adatom. The decrease in currents was observed as

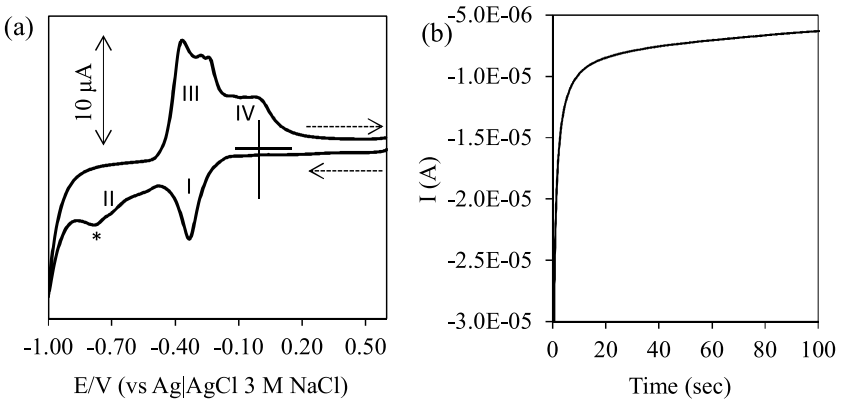


**Fig. 1.** (a) Cyclic voltammogram of gold electrode measured between 0.60 V to -1.0 V in pH 4.0 acetate buffer solution containing 1.0 mM $Ni(NO_3)_2.H_2O$ and (b) chronoamperommo-gram for the electrodeposition of Ni(0) onto gold electrode surface, $E_{app}$ = -0.80 V.

the deposition of nickel continued. This observed phenomenon was a clear indication that nickel metal thin film was electrodeposited. The formation of Ni thin film reached saturation after 100 s forming Au-Ni thin film. The monolayer of Ni is first deposited during the adatom formation, however multiple layers were deposited as the electrodeposition proceeded until 100 s.

The Au-Ni thin film deposited was confirmed by scanning the modified electrode in alkaline solution containing sodium hydroxide. Fig. 2 shows the cyclic voltammogram (CV) of Au-Ni measured in 0.10 M NaOH. The multiple scans were measured and the stable 10th scan is shown in Fig. 2. The electrodeposited Au-Ni thin film was electrochemically converted to the electrocatalytic active Au-NiO/$Ni(OH)_2$ using multiple scans in alkaline solution (0.10 M NaOH). Two redox couples were observed and the peaks are labelled (**I**) and (**II**) with half-wave potential ($E_{½}$) of 0.190 V ($NiO + OH^- \leftrightarrow NiOOH + e^-$) and 0.260 V ($NiOOH + OH^- \leftrightarrow Ni(OH)_2 + H_2O + e^-$) respectively. The observed redox peaks are due to the reversible Ni oxidation and reduction in alkaline conditions [30].

The electrodeposition resulted in NiO/$Ni(OH)_2$ thin film on the gold electrode surface. The observed cyclic voltammograms were also similar to the reported powder electrochemical NiO prepared using conduit synthesis technology [28]. Zhang et al. [28] concluded that this is a single redox peak even though the CV showed two redox processes. In this study, the two redox peaks were clearly observed and due to nickel oxide to nickel oxy-hydroxide and the second redox peak was due to the nickel oxy-hydroxide to nickel hydroxide.

During the anodic and cathodic scans for nickel hydroxide electrode surface four possible phases are possible, that is, β-$Ni(OH)_2$, α-$Ni(OH)_2$, γ-NiOOH and β-NiOOH. The formation of γ-NiOOH is associated with swelling or volume expansion of nickel films onto gold electrodes with microcracks and disintegration may occur. Therefore, β-NiOOH and β-$Ni(OH)_2$ phases are expected to give better electroactive material for high electrochemical performance in alkaline medium [12,22]. During the multiple scans, the redox couple showed an increase in current and this is attributed to the increase in electrochemical conductivity of the formed thin film as previously reported [12]. After the 10th scan, the scan was stable and the formed thin film was represented as Au-NiO/$Ni(OH)_2$. The Au-NiO/$Ni(OH)_2$ thin film provides a good adsorption surface for GOx enzyme via hydrogen bonding and allowing the enzyme to retain its natural activity thus promoting excellent enzyme-substrate interaction [39]. The GOx enzyme immobilization was achieved by electrodeposition. The potential ($E_{app}$) of +0.80 V (vs Ag|AgCl, 3 M NaCl) was applied for the electrodeposition of 5.0 µg.$mL^{-1}$ of GOx in 2.0 mL pH 7.4 PBS solution. Fig. 3 shows the chronoamperommogram for the electrodeposition of GOx enzyme. The GOx enzyme electrodeposition took 300 s and stable current was observed. The percentage relative standard deviation (% RSD) for the adsorption of Au-Ni adatom, its conversion into Au-NiO/$Ni(OH)_2$ and immobilization of GOx (Au-NiO/$Ni(OH)_2$-GOx) was < 5 % for triplicate measurements. The established modification protocol clearly shows excellent reproducibility and control with minor or negligible experimental errors.

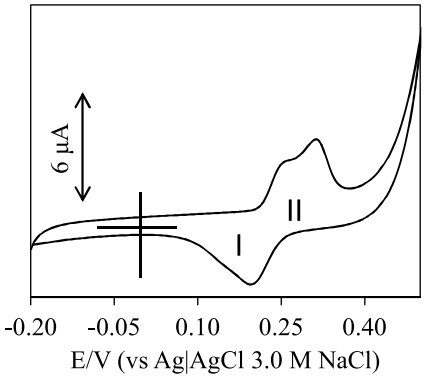


**Fig. 2.** Cyclic voltammogram (stable 10th scan) of Au-Ni in 0.10 M NaOH solution at scan rate of 50 mV $s^{-1}$.

### 3.2. Surface analysis and characterization of the gold electrode modification

The step-by-step characterization of the bare Au, Au-NiO/$Ni(OH)_2$ and Au-NiO/$Ni(OH)_2$-GOx surfaces was studied. The surface sensitive techniques such as cyclic voltammetry, time-of-fight secondary ion mass spectroscopy (TOF-SIMS) and X-ray photoelectron spectroscopy (XPS) were used for surface analysis. Fig. 4 shows the cyclic voltammograms (CVs) of (i) bare Au, (ii) Au-NiO/$Ni(OH)_2$ and (iii) Au-NiO/Ni$(OH)_2$-GOx surfaces measured in 2.0 mM $K_3/K_4[Fe(CN)_6]$ containing 0.10 M KCl.

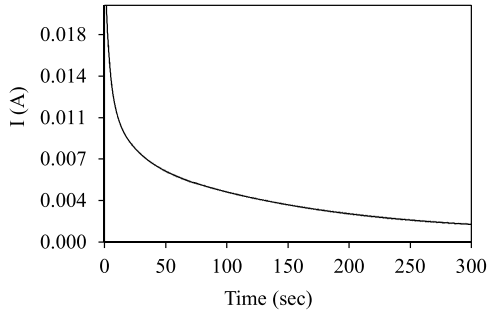


**Fig. 3.** The electrodeposition of 5.0 µg.$mL^{-1}$ GOx enzyme from 1.0 mM PBS (pH 7.4) solution and $E_{app}$ = +0.80 V (vs Ag|AgCl 3 M NaCl) at Au-NiO/Ni$(OH)_2$ electrode.

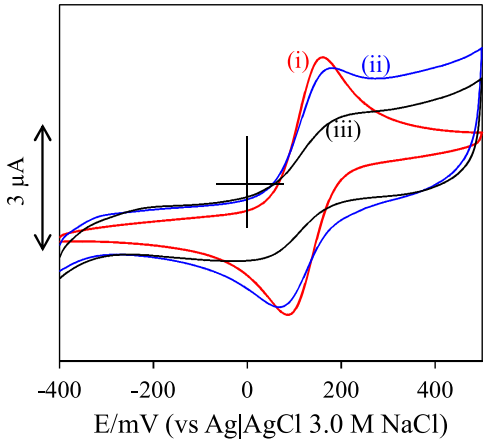


**Fig. 4.** Cyclic voltammograms of bare (i) Au, (ii) Au-NiO/Ni(OH)$_2$ and Au-NiO/Ni(OH)$_2$-GOx in 2.0 mM $K_3/K_4[Fe(CN)_6]$ containing 0.10 M KCl (pH 7.0).

At the bare or unmodified electrode surfaces, Fig. 4(i), a reversible redox couple, the $[Fe(CN)_6]^{3-/4-}$, was observed with a peak-to-peak potential separation (ΔE) of 71 ± 5.0 mV. The ideal value for a one electron process is 59 mV, however a value of 71 ± 5.0 mV is acceptable for unmodified gold electrode surfaces. A thin film may present different properties on the gold electrode. For an example, if the thin film is an insulator, a decrease in peak current densities and increase in peak-to-peak (ΔE) separation will occur. The opposite will occur for a conducting thin film [40,41]. Using $[Fe(CN)_6]^{3-/4-}$ as a redox probing species, the modification and deposition of thin films and its properties can be monitored. After electrodeposition and formation of the Au-NiO/Ni(OH)$_2$ ΔE increased to 104 ± 3.0 mV. There was an observed shift in the oxidation peak to higher potential values and reduction peak to lower potential values. The peak currents decreased whilst ΔE increased from 71 ± 5.0 mV to 104 ± 3.0 mV. The Au-NiO/Ni(OH)$_2$ is conducting hence the observed redox couple due to the $[Fe(CN)_6]^{3-/4-}$. There was a slight decrease in peak current density due to the slight inhibition of the redox species due to the oxo-hydroxyl surface with δ- charge repelling the negatively charged $[Fe(CN)_6]^{3-/4-}$ redox species. After electrodeposition of GOx, a drastic decrease in the current density was observed and due to the insulating glycoprotein of the GOx enzyme. The ΔE after GOx electrodeposition increased further from 104 ± 3.0 mV for Au-NiO/Ni(OH)$_2$ to 254 ± 20 mV for Au-NiO/Ni(OH)$_2$-GOx. The glycoprotein of GOx behaves like a barrier for electron transfer and the redox process. In addition to the decrease in current and increase in ΔE, there was an increase in capacitive currents at the potentials < 0 mV and also above 300 mV in both Au-NiO/Ni(OH)$_2$ and Au-NiO/Ni(OH)$_2$-GOx. The capacitive properties of NiO/Ni(OH)$_2$ has been reported before for platelets chemically synthesized [24–31]. The electrochemical studies confirmed the electrodeposition of NiO/Ni(OH)$_2$ and GOx enzyme thin films onto gold electrode.

In addition to the electrochemical characterization, the electrode modification was confirmed using XPS. Fig. 5 shows the (a) XPS survey spectra and (b) Ni 2p high-resolution spectra of (i) Au, (ii) Au-NiO/Ni(OH)$_2$ and (iii) Au-NiO/Ni(OH)$_2$-GOx electrodes. The survey spectra showed the elemental composition of the bare and modified electrodes with NiO/Ni(OH)$_2$ and GOx. The observed elements and their binding energy positions were O 1s (532 eV), Au 4d (334 eV), C 1s (285 eV), N 1s (398 eV) and Au 4f (84 eV).

Fig. 5(a)(i), for a bare Au exhibited the presence of Au 4f, Au 3d, C 1s and O 1s. The presence of gold was due to the gold coated quartz crystal surface used. The carbon (C 1s) and oxygen (O 1s) were due to exposure of bare gold surface to absolute ethanol during the pre-treatment of gold crystal and exposure to air before the analysis. The survey spectrum of Au-NiO/Ni(OH)$_2$ in Fig. 5(a)(ii) showed the presence of Ni 2p peak at 848 eV. The Ni 2p peak was not observed at bare Au and GOx modified gold (Au-NiO/Ni(OH)$_2$-GOx) surfaces, in Fig. 5(a)(iii). The disappearance of the Ni 2p peak at Au-NiO/Ni(OH)$_2$-GOx was attributed to the GOx glycoprotein covering the underlying nickel oxide surface. The Au-NiO/Ni(OH)$_2$-GOx surface also showed an additional N 1s peak. The presence of the N 1s was of high significance as it confirmed the adsorbed GOx enzyme. It was interesting to observe the presence of gold but this was attributed to the abundance of gold as the bulk surface. From the survey spectra we also observed the increase in the peak intensity for C 1s and O 1s from bare Au to Au-NiO/Ni(OH)$_2$ and to Au-NiO/Ni(OH)$_2$-GOx. The increase in the peak intensity was attributed to the immobilization with carbon and oxygen containing materials. Fig. 5(b) shows the high-resolution spectra of Ni 2p which clearly confirmed the immobilization of NiO/Ni(OH)$_2$ and GOx thin films onto gold surface. At Au-NiO/Ni(OH)$_2$ surface in Fig. 5(b)(ii), the Ni $2p_{3/2}$ and Ni $2p_{1/2}$ orbit-split coupling components were observed and deconvoluted to multiple components. The spin-orbit coupling (ΔE) for the two corresponding components was ~18 eV. The high resolution Ni 2p peak showed both the primary ion and the corresponding shake-up or satellite peaks for both Ni $2p_{3/2}$ and Ni $2p_{1/2}$ components. The satellite peaks were observed at high binding energies than their corresponding primary peaks. The Ni 2p spectrum did not show peaks due to $Ni^0$ which appears at 852.6 eV. Majority of the peaks were observed at binding energies for NiO (853.4 eV) and Ni(OH)$_2$ (855.2 eV). The oxidation state of nickel was confirmed to be Ni (II). The high resolution core-level spectra of C 1s and O1s were also analysed and discussed in Fig. S1 (ESI).

The survey spectra were quantified by estimating the chemical composition of the elements obtained from the surfaces. The respective atomic concentrations are summarized in Table S1. The bare Au exhibited four elements, namely O 1s (9.3 %), C 1s (46.8 %) and Au 4f (43.9 %). Upon modifying the electrode with NiO/Ni(OH)$_2$ thin film, the atomic concentration of oxygen increase from 9.3 % to 17.0 % and due to interstitial (Ni-O-Ni), oxide (Ni-O) and hydroxide (−OH) oxygen. The oxygen increased slightly after GOx deposition to 17.8 % due to the glycoprotein of GOx enzyme. The C 1s atomic percentage composition of 46.8 % decreased slightly to 43.3 % from Au and Au-NiO/Ni(OH)$_2$ surfaces. The C 1s for Au-NiO/Ni(OH)$_2$-GOx surface increased from 43.3 % to 56.6 % confirmed the immobilization of the carbon-rich GOx enzyme. The atomic percentage composition of Au 4f showed a decreasing trend from 43.9 % > 34.5 % > 18.1 % for bare Au > Au-NiO/Ni(OH)$_2$ > Au-NiO/Ni(OH)$_2$-GOx surfaces. The decrease in Au 4f was due to the NiO/Ni(OH)$_2$ and NiO/Ni(OH)$_2$-GOx thin films and blocking the underlying Au surface. The Au-NiO/Ni(OH)$_2$ surface showed Ni 2p present with 5.2 % and is not observed on the bare Au in Fig. 5(b)(i) and Au-NiO/Ni(OH)$_2$-GOx in Fig. 5(b)(iii). At the Au-NiO/Ni(OH)$_2$-GOx, N 1s with a percentage composition of 5.5 % was observed and confirmed the presence of GOx and due to the glycoprotein.

In addition to the XPS method discussed above and in the Electronic Support Information (**ESI**), other surface techniques were studied. The morphology and surface roughness of the bare Au, Au-NiO/Ni(OH)$_2$ and Au-NiO/Ni(OH)$_2$-GOx was investigated using Atomic Force Microscope (AFM) in Fig. S2 (ESI). In addition to the morphology (discussed in the ESI), the roughness factor (RMS) increased from 1.24 nm for bare Au to 1.60 nm for Au-NiO/Ni(OH)$_2$ and to 2.21 nm for Au-NiO/Ni(OH)$_2$-GOx. Time-of-flight secondary ionization mass spectrometry (TOF-SIMS) in Fig. S3 (ESI) was also used to investigate each of the film thickness. The film thickness was confirmed to be 10 nm for NiO/Ni(OH)$_2$ and 20 nm for GOx in Au-NiO/Ni(OH)$_2$-GOx surface following the $Ni^+$ molecular ion ($m/z$) of 57.93 and molecular ion ($m/z$) of 119.93 in positive mode. The detailed discussion of the AFM and TOF-SIMS results is in the ESI.

### *3.3. Electrocatalysis and bioelectrocatalysis of bare and modified gold surfaces*

The first investigation involved the detection of hydrogen peroxide

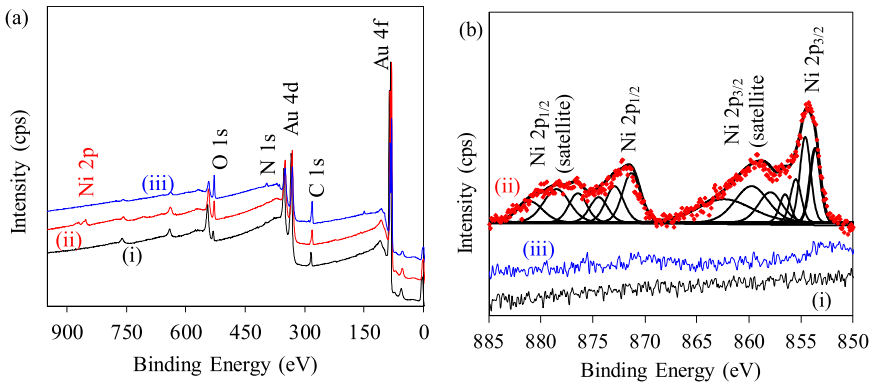


**Fig. 5.** XPS (a) survey spectra and (b) the high-resolution core level spectra of Ni 2p for (i) Au, (ii) Au-NiO/Ni(OH)$_2$ and (iii) Au-NiO/Ni(OH)$_2$-GOx surfaces.

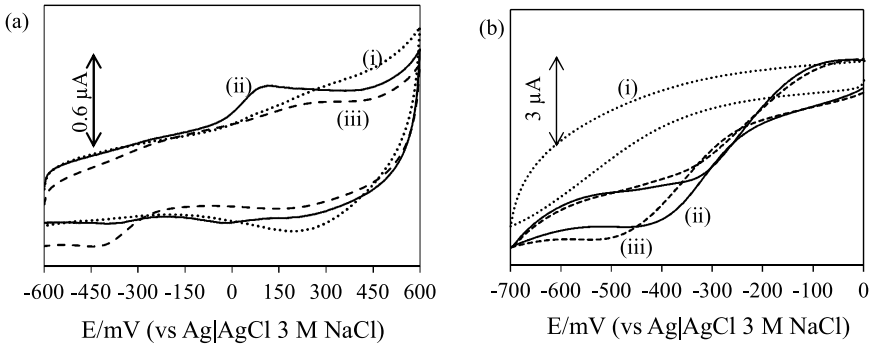


**Fig. 6.** Cyclic voltammograms of (i) bare Au, (ii) Au-NiO/Ni(OH)$_2$ and (iii) Au-NiO/Ni(OH)$_2$-GOx in (a) pH 7.4 PBS and (b) pH 7.4 PBS + 0.10 mM $H_2O_2$. Scan rate = 50 mV $s^{-1}$.

as a by-product of glucose oxidase enzyme. The electrochemical properties of the different electrode surfaces were investigated by cyclic voltammograms in phosphate buffer solution (PBS, pH 7.4). Fig. 6 shows cyclic voltammograms of (i) bare Au, (ii) Au-NiO/Ni(OH)$_2$ and (iii) Au-NiO/Ni(OH)$_2$-GOx in (a) pH 7.4 PBS and (b) pH 7.4 PBS + 0.10 mM $H_2O_2$. The solution (pH 7.4 PBS + 0.10 mM $H_2O_2$) was deaerated with argon (Ar) to remove dissolved oxygen and the electrochemical cell was kept under argon atmosphere. There were no redox peaks observed for the bare Au electrode surface in Fig. 6(a)(i). The Au-NiO/Ni(OH)$_2$ surface showed a redox peak $E_{½}$ at 50 mV and corresponds to $Ni^{II}/Ni^{I}$ in Fig. 6(a)(ii). After the electrodeposition of GOx enzyme, the $Ni^{II}/Ni^{I}$ redox was buried under the glycoprotein and the new redox peak at $E_{½}$ of −318 mV in Fig. 6(a)(iii) was observed and due to the enzyme co-factor (FAD/$FADH_2$) [1]. The amount of GOx enzyme deposited was determined by integrating the charge (Q = 0.368 µF) under the reduction peak and the surface coverage was found to be 1.43 × $10^{-10}$ mol. $cm^{-2}$. It was interesting to observe this redox peak from the GOx enzyme and confirms the conducive and optimum enzyme orientation onto Au-NiO/Ni(OH)$_2$ surface [10,13]. This confirms that the GOx enzyme co-factor is oriented towards the electrode surface and thus leaving the glucose binding site facing the solution. The orientation of the enzyme is one of the most important aspect of biosensor design. The obtained orientation will allow for the strong interaction between the GOx enzyme and the glucose substrate (as the analyte). In the presence of 0.10 mM $H_2O_2$ in Fig. 6(b)(i), the bare gold showed an increase in current but there was no peak due to the electrocatalytic reduction of $H_2O_2$. The Au-NiO/Ni(OH)$_2$ in Fig. 6(b)(ii), the electroreduction occurred with the onset potential at -200 mV and the peak was observed at −447 mV. The highly inclined slope from the onset potential (−200 mV) confirmed the excellent electrocatalysis of Au-NiO/Ni(OH)$_2$ towards $H_2O_2$. At Au-NiO/Ni(OH)$_2$-GOx, a peak due to $H_2O_2$ was observed at −525 mV with slightly delayed onset potential at −254 mV. The delayed onset and the shift of $H_2O_2$ electrocatalytic reduction peak at Au-NiO/Ni(OH)$_2$-GOx is due to the sluggish diffusion of $H_2O_2$ through the GOx glycoprotein. The electroreduction of $H_2O_2$ on both the Au-NiO/Ni(OH)$_2$ and Au-NiO/Ni(OH)$_2$-GOx occurs at the NiO/Ni(OH)$_2$ thin film due to the almost similar electrocatalytic potentials and electrocatalytic currents. The $Ni^{II}/Ni^{I}$ redox peak which was observed in Fig. 2 is involved in the electrocatalytic reduction of $H_2O_2$. The NiO/Ni(OH)$_2$ are already in +2 oxidation state as confirmed by XPS and hence the reduction due to $Ni^{II}/Ni^{I}$.

The electrococatalytic detection of glucose at the various electrode surfaces was investigated. Fig. 7 shows the cyclic voltammogram of (i) bare Au, (ii) Au-NiO/Ni(OH)$_2$ and (iii) Au-NiO/Ni(OH)$_2$-GOx in 2.0 mM glucose in PBS pH 7.4. Argon was bubbled into a PBS substrate solution (pH 7.4) containing 2.0 mM glucose and a blanket of argon was kept over the electrochemical cell to prevent the oxygen interference. The bare Au in Fig. 7(i) and Au-NiO/Ni(OH)$_2$ in Fig. 7(ii) both did not show the peak due to the presence of glucose. There was an increase in electrocatalytic currents at Au-NiO/Ni(OH)$_2$. At Au-NiO/Ni(OH)$_2$-GOx

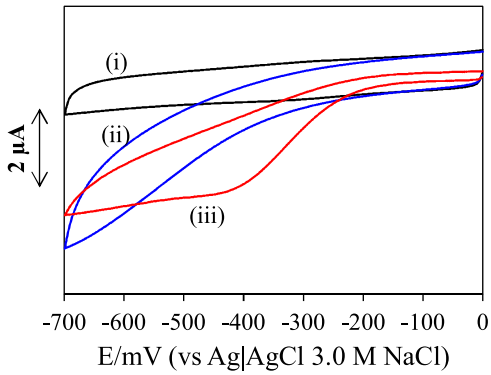


**Fig. 7.** Cyclic voltammograms of (i) bare Au, (ii) Au-NiO/Ni(OH)$_2$ and (iii) Au-NiO/Ni(OH)$_2$-GOx in 2.0 mM glucose in PBS pH 7.4.

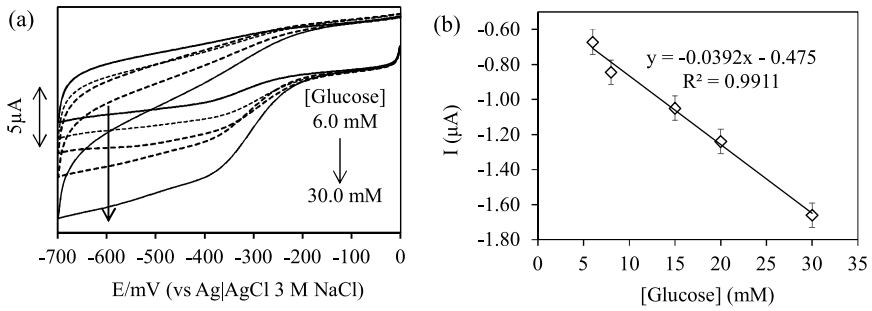


**Fig. 8.** (a) Cyclic voltammograms and (b) calibration curve for Au-NiO/Ni(OH)$_2$-GOx at different concentrations of glucose ranging from 6.0 mM, 8.0 mM, 15.0 mM, 20.0 mM, and 30.0 mM in 0.050 M PBS (pH 7.4) solution. The current for the calibration curve was sampled at -600 mV. % RSD < 5% for n = 3.

surface, in Fig. 7(iii), the electrocatalytic current increased and the onset potential was at -200 mV and the current increased up until the peak at −454 mV was obtained and due to the electrocatalytic reduction of $H_2O_2$ as GOx enzyme by-product. The electrocatalytic reduction potential was similar to that of Au-NiO/Ni(OH)$_2$ electrode above for $H_2O_2$. The monitoring of $H_2O_2$ production or $O_2$ consumption can be used for the GOx enzyme – glucose detection and platinum is an electrode material of choice for such a reaction. Platinum is a rare platinum group metal whilst gold electrodes are widely available at relatively affordable cost. Gold electrode was chosen for this work due to the known copper under-potential deposition (CuUDP). NiUDP was used in this work for Au-NiO/Ni(OH)$_2$ electrode fabrication. The production of $H_2O_2$ was monitored and this resulted in the increase in electrochemical reduction signal due to the increase in glucose concentration. The modification of gold electrode was achieved within a few minutes and thus making the Au-NiO/Ni(OH)$_2$ suitable substitute for the expensive platinum for $H_2O_2$ detection.

The electroanalysis of glucose onto Au-NiO/Ni(OH)$_2$-GOx surface was investigated. Fig. 8 shows the cyclic voltammograms of Au-NiO/Ni(OH)$_2$-GOx surface at different concentrations (6.0 mM, 8.0 mM, 15.0 mM, 20.0 mM, and 30.0 mM) of glucose in 1.0 mM PBS (pH 7.4) solution. There was an increase in electrocatalytic currents upon increasing glucose concentrations in Fig. 8(a). This was attributed to the glucose oxidation by GOx enzyme producing $H_2O_2$ which was electrocatalytical reduced to $H_2O + O_2$ at Au-NiO/Ni(OH)$_2$ hence the increase in electrocatalytic currents. The linear calibration plot was obtained for electrocatalytic current against glucose concentration in Fig. 8(b). The linear concentration range of glucose was within the clinical relevant range for monitoring glucose by patients with diabetes. The regression coefficient ($R^2$) was obtained to be 0.99. The mechanism of bioelectrocatalysis is shown and discussed in Scheme S1 (ESI). The relative standard deviation (% RSD) of the Au-NiO/Ni(OH)$_2$-GOx was conducted in triplicates and the deviation was < 5 % as shown in Fig. 8(b) confirming excellent reproducibility. The limit of detection (LoD) using signal to noise ratio of 3 was calculated to be 1.54 ± 0.03 mM. The sensitivity of the biosensors was 1.95 ± 0.13 μA.mM.cm$^{-2}$. The selectivity was also evaluated using ascorbic acid and uric acid both in solution and at modified surface. There was no significant signal generated by 1.0 mM ascorbic acid and uric acid confirming the selectivity and specificity of GOx both in solution and immobilized on the surface (Au-NiO/Ni(OH)$_2$-GOx). This confirmed that the biosensor could detect only D-glucose due to glucose oxidase enzyme.

## 4. Conclusions

The gold electrode was successfully modified, using the electrodeposition method, with the thin films of NiO/Ni(OH)$_2$ and GOx enzyme. The electrodeposition was followed using several surface sensitive techniques which confirmed the successful modification of gold with NiO/Ni(OH)$_2$ and GOx thin films. The cyclic voltammetry confirmed the electrocatalytic properties of NiO/Ni(OH)$_2$ thin film towards $H_2O_2$. The XPS, AFM and TOF-SIMS surface sensitive techniques confirmed the electrodeposition of NiO/Ni(OH)$_2$ and GOx thin films onto gold surface. The XPS results confirmed the formation of NiO/Ni(OH)$_2$ thin films with a Ni 2p high-resolution and a +2 oxidation state. The presence of the GOx was confirmed by the quantitative increase in at % for the C 1s and the presence of N 1s. The AFM exhibited an increase in roughness factor (RMS) and the morphology of the images also confirmed the electrodeposited NiO/Ni(OH)$_2$ and GOx thin films. The TOF-SIMS, depth-profiling confirmed the electrodeposition of 10 nm NiO/Ni(OH)$_2$ thin films and the 20 nm GOx thin films. The Au-NiO/Ni(OH)$_2$ and Au-NiO/Ni(OH)$_2$-GOx electrodes could detect 0.10 mM $H_2O_2$ with electrocatalytic reduction peak at −447 mV and −525 mV. The Au-NiO/Ni(OH)$_2$-GOx was investigated for the detection of glucose with success. An increase in the electrocatalytic reduction currents was observed at different glucose concentrations and was linear up to 30 mM in 1.0 mM PBS (pH 7.4). The Au-NiO/Ni(OH)$_2$ thin film allowed for oriented electrodeposited of GOx with excellent electron transfer properties. A redox couple of GOx in pH 7.4 was observed at $E_{½}$ of −454 mV and due to direct electron transfer of the enzyme co-factor, FAD/FADH$_2$.

## CRediT authorship contribution statement

**Nqobile Njoko:** Conceptualization, Data curation, Validation, Investigation, Writing - original draft. **Marcel Louzada:** Data curation, Investigation, Methodology. **Jonathan Britton:** Data curation, Investigation, Methodology. **Samson Khene:** Methodology, Formal analysis, Writing - review & editing, Methodology. **Tebello Nyokong:** Resources, Funding acquisition, Writing - review & editing, Writing - original draft. **Philani Mashazi:** Conceptualization, Supervision, Data curation, Formal analysis, Funding acquisition, Investigation, Methodology, Resources, Writing - original draft, Writing - review & editing, Validation.

## Declaration of Competing Interest

The authors declare that they have no known competing financial interests or personal relationships that could have appeared to influence the work reported in this paper.

## Acknowledgements

This work was supported by the South African Medical Research Council under a Self-Initiated Research Grant (MRC-SIR); National Research Foundation through Thuthuka Post-PhD Programme (UID 84223), Rated Incentive funding (UID 96001) and Rhodes University Research Council, Researcher Development Grant (RDG P5/17/2015). NN thanks Moshal for BSc Honours Scholarship.

## Appendix A. Supplementary data

Supplementary material related to this article can be found, in the online version, at doi:https://doi.org/10.1016/j.colsurfb.2020.110981.

## References


[1] C. Qiu, X. Wang, X. Liu, S. Hou, H. Ma, Electrochim. Acta 67 (2012) 140.
[2] L. Özcan, Y. Şahin, H. Türk, Biosens. Bioelectron. 24 (2008) 512.
[3] J.S. Skyler, I.A. Lasky, D.L. Skyler, E.G. Robertson, D.H. Mintz, Diabetes Care 1 (1978) 150.
[4] K. Rajpoot, Biosens. J. 6 (2017) 145.
[5] L.M. Welschen, E. Bloemendal, G. Nijpels, J.M. Dekker, R.J. Heine, W.A. Stalman, L.M. Bouter, Diabetes Care 28 (2005) 1510.
[6] S. Martin, B. Schneider, L. Heinemann, V. Lodwig, H.J. Kurth, H. Kolb, W.A. Scherbaum, Diabetologia 49 (2006) 271.
[7] W.A. Davis, D.G. Bruce, T.M. Davis, Diabetes Care 29 (2006) 1764.
[8] J. Wang, Chem. Rev. 108 (2008) 814.
[9] N.S. Oliver, C. Toumazou, A.E.G. Cass, D.G. Johnston, Diabet. Med. 26 (2008) 197.
[10] A. Salimi, E. Sharifi, A. Noorbakhsh, S. Soltanian, Biosens. Bioelectron. 22 (2007) 3146.
[11] A.A. Saei, J.E.N. Dolatabadi, P. Najafi-Marandi, A. Abhari, M. de la Guardia, TrAC 42 (2013) 216.
[12] A.M. Ghonim, B.E. El-Anadouli, M.M. Saleh, Electrochim. Acta 114 (2013) 713.
[13] C.X. Guo, C.M. Li, Phys. Chem. Chem. Phys. 12 (2010) 12153.
[14] M. Velmurugan, S. Sakthinathan, S.-M. Chen, C. Karuppiah, Int. J. Electrochem. Sci. 10 (2015) 6663.
[15] Y. Yu, Z. Chen, S. He, B. Zhang, X. Li, M. Yao, Biosens. Bioelectron. 52 (2014) 147.
[16] M. Wooten, S. Karra, M. Zhang, W. Gorski, Anal. Chem. 86 (2014) 752.
[17] S. Schleev, A. Jarosz-Wilkolazka, A. Khalunina, O. Morozova, A. Yaropolov, T. Ruzgas, L. Gorton, Bioelectrochem. 67 (2005) 115.
[18] J. Martinez-Ortiz, R. Flores, R. Vazquez-Duhalt, Biosens. Bioelectron. 26 (2011) 2626.
[19] X.-H. Zhou, X.-R. Huang, L.-H. Liu, X. Bai, H.-C. Shi, RSC Adv. 3 (2013) 18036.
[20] R.S. Freire, C.A. Pessoa, L.D. Mello, L.T. Kubota, J. Braz. Chem. Soc. 14 (2003) 230.
[21] S.K. Arya, S. Saha, J.E. Ramirez-Vick, V. Gupta, S. Bhansali, S.P. Singh, Anal. Chim. Acta 737 (2012) 1.
[22] S.M. El-Refaei, M.I. Awad, B.E. El-Anadouli, M.M. Saleh, Electrochim. Acta 92 (2013) 460.
[23] D. Mohammadyani, S.A. Hosseini, S.K. Sadrnezhaad, Int. J. Modern Phys.: Conf. Series 5 (2012) 270.
[24] X. Liu, L. Yu, J. Power Sources 128 (2004) 326.
[25] X.J. Han, P. Xu, C.Q. Xu, L. Zhao, Z.B. Mo, T. Liu, Electrochim. Acta 50 (2005) 2763.
[26] D. Yang, R. Wang, M. He, J. Zhang, Z. Liu, J. Phys. Chem. B 109 (2005) 7654.
[27] G. Xiao-Yan, D. Jiang-Cheng, Mater. Lett. 61 (2007) 621.
[28] W. Zhang, W. Jiang, L. Yu, Z. Fu, W. Xia, M. Yang, Int. J. Hydrogen Energy 34 (2009) 473.
[29] T.N. Ramesh, Mater. Chem. Phys. 114 (2009) 618.
[30] M.-S. Wu, H.-H. Hsieh, Electrochim. Acta 5 (2008) 3427.
[31] B. Li, M. Ai, Z. Xu, Chem. Comm. (2010) 6267.
[32] A. Vaskevich, F. Sinapi, Z. Mekhalif, J. Delhalle, I. Rubinstein, J. Electrochem. Soc. 152 (2005) C744.
[33] D. Mwanza, S. Mvango, S. Khene, T. Nyokong, P. Mashazi, Electrochim. Acta 254 (2017) 89.
[34] S.N. Nxele, P. Mashazi, T. Nyokong, Electroanalysis 27 (2015) 2468.
[35] Z.O. Makinde, M. Louzada, P. Mashazi, T. Nyokong, S. Khene, Appl. Surf. Sci. 425 (2017) 702.
[36] NIST (National Institute of Standards and Technology), X-ray Photoelectron Spectroscopy Database, NIST Standard Reference Database Number 20, National Institute of Standards and Technology, Gaithersburg MD, 2000, p. 20899 doi:10.18434/T4T88K, retrieved [21 May 2018].
[37] M. Managa, B.P. Ngoy, D. Mafukidze, J. Britton, T. Nyokong, J. Photochem. Photobio. A: Chem. 348 (2017) 179.
[38] G.L. Borges, K.K. Kanazawa, J.G. Gordon II, K. Ashley, J. Richer, J. Electroanal. Chem. 364 (1994) 281.
[39] J. Zdarta, A.S. Meywe, T. Jesionowski, M. Pinelo, Catalysis 8 (2018) 92.
[40] P. Mashazi, P. Tetyana, S. Vilakazi, T. Nyokong, Biosens. Bioelectron. 49 (2013) 32.
[41] P. Mashazi, T. Mugadza, N. Sosibo, P. Mdluli, S. Vilakazi, T. Nyokong, Talanta 85 (2011) 2202.